Polymer Diffusion in Semicrystalline Polymers Using Secondary Ion Mass Spectroscopy

Rachel A. Segalman,† Aaron Jacobson,‡ and Edward J. Kramer*

Chemical Engineering and Materials Departments, University of California, Santa Barbara, Santa Barbara, California 93106

Steven R. Lustig

Central Research Division, E. I. Dupont de Nemours & Co., Inc., Experimental Station, Route 141, Wilmington, Delaware 19880-0356

Received November 12, 2003; Revised Manuscript Received February 4, 2004

ABSTRACT: The diffusion of deuterium-labeled atactic polystyrene (dPS) from the surface of a precrystallized polydisperse, isotactic polystyrene (iPS) matrix was measured using dynamic secondary ion mass spectroscopy (DSIMS). The detailed depth profiles indicated two types of mass transport into the iPS matrix. A layer near the surface of the film was observed to fit a Gaussian function whose prefactor decreased with diffusion time but whose width increased only very slowly with diffusion time. An underlying profile was observed to correspond to Fickian diffusion from a constant composition, C_0, of dPS at the interface with the surface layer into the underlying iPS. The concentration, C_0, decreased with increasing dPS degree of polymerization, N, and appears to be the saturation concentration at the surface of the iPS layer. The tracer diffusion coefficient, D, extracted from the underlying diffusion profile decreased as N^{-1}. This N dependence is suggestive of entropic barrier type diffusion.

Introduction

Polymer diffusion into semicrystalline polymers at temperatures below the melting point of the crystal provides fundamental information concerning the dynamics of chains within the amorphous regions between the crystals, regions expected to have a complex morphology. This diffusion of chains into these complex structures is not well understood despite the impact this phenomenon has on a variety of engineering applications such as crack healing and welding.

In general, the diffusion of a small molecule penetrant into a semicrystalline matrix has been observed to have non-Fickian overall kinetics.[1−4] In particular, Quijada-Garrido et al.[4] propose a semiempirical dual mechanism for the diffusion of small molecules into a semicrystalline matrix. They observed two simultaneous Fickian processes, one dominating near the source as the matrix is saturated and another much slower mechanism as the tracer filters through the bottlenecks between crystallites. Fewer studies exist characterizing the diffusion of a polymeric tracer into a semicrystalline matrix. Billingham et al.[5] noted that the diffusion of atactic polymer chains into a polymeric matrix is quite different than the diffusion of small additive molecules. In particular, the diffusion of atactic polypropylene into a crystallizing matrix is characterized by the rejection of the atactic polymer from the crystallizing regions.

Similar diffusion experiments were conducted by Van Alsten et al.[1] for the diffusion of atactic polystyrene tracers into a precrystallized isotactic polystyrene matrix. Using an infrared ATR spectroscopy technique, Van Alsten et al. observed that imbibation rates appear to be Fickian at short diffusion times, but found a deviation from Fickian diffusion kinetics at later diffusion times. The infrared technique measures the amount of polymer that has diffused away from the tracer layer and into the matrix. In this manner, infrared ATR spectroscopy gives a quantitative measure of the amount of polymer imbibed by the matrix and has proved to be extremely useful in measuring diffusion coefficients. This method, however, is not capable of monitoring the detailed progress of chains into the matrix via a depth profile. The imbibition information suggests that at early times mutual diffusion occurs to saturate the amorphous pockets of the matrix after which tracer molecules explore the bottlenecks between crystalline obstacles, a process which was characterized by a transition to a much slower diffusion regime. Furthermore, the diffusion coefficient did not appear to follow the power law dependence on tracer size (N) predicted by reptation or Rouse diffusion. Instead, as the tracer size was increased, they observed that the dependence of D on N weakened significantly.

The diffusion of the chain through a series of bottlenecks may be controlled by the entropic barrier associated with the chain deforming to pass through a spatial constraint.[6−9] The number of accessible configurations available at each position defines the local entropy of the molecule. The spatial heterogeneity of the matrix causes chains to collect in less constricted regions. Diffusion occurs as the chain segments jump across the intervening barriers. Muthukumar and Baumgartner[6] first modeled the diffusion of chains through a periodic array of cubic cavities and found that the diffusion coefficient was smaller than that of an unimpeded, unentangled chain, the Rouse diffusion coefficient. They then used Monte Carlo simulations to explore this diffusion mechanism with a self-avoiding walk chain which performs Brownian motion between randomly distributed obstacles.[7] Their results suggest that at very short diffusion times Rouse dynamics should be ob-

† Present address: Department of Chemical Engineering, 201 Gilman Hall, University of California, Berkeley, Berkeley, CA 94720-1462.

‡ Present address: South High School, Bakersfield, CA.

* To whom correspondence should be addressed: Tel (805)893-4999; e-mail edkramer@mrl.ucsb.edu.

10.1021/ma035705a CCC: $27.50
Published on Web 03/13/2004

served as the chains move over distances smaller than the average separation between obstacles. At later times, diffusivity is described by the partitioning of the chain between the bottlenecks and open pockets. This diffusion coefficient, D, is described by

$$\frac{D}{D_0} = \exp\left(-N\left[f\left(\frac{1}{C}\right)^{1/\nu} + \left(\frac{1-f}{z} - 1\right)\left(\frac{1}{C_1}\right)^{1/\nu}\right]\right) \quad (1)$$

where D_0 is the Rouse diffusion coefficient (in the absence of obstacles), ν is the exponent relating the radius of gyration of the chain and N, f is the ratio of bottleneck length to that necessary to enclose the entire chain (of length N), z is the number of open domains per bottleneck, C is the cross section of the bottleneck, and C_1 is the average pocket size. When the chains are much longer than the bottlenecks ($f \ll 1$), $f \sim N^{-1}$. For small values of C, the first term in the square brackets (which is independent of N) dominates. In this case, D follows the same N dependence as D_0 so $D \sim N^{-1}$ but $D \ll D_0$.

Nykypanchuk et al. have directly visualized the diffusion of linear DNA molecules within a two-dimensional array of spherical cavities connected by circular holes.[10] The holes acted as entropic barriers, and the expected chain length dependence of $D \sim N^{-1}$ was again observed. It has been postulated, however, that entropic barrier diffusion only occurs in a molecular weight window in which the polymer chain must squeeze through dense regions in the matrix. If the tracer chains are shorter, they will not be affected by the randomness of the confinement. If the molecular weight of the tracer is much larger and the chain is highly entangled, it will respond to an averaged environment instead of to individual obstacles and reptation dynamics will be observed.[11]

Recently, dynamic secondary ion mass spectroscopy (SIMS) has been used to better understand complex diffusion mechanisms by generating detailed depth profiles of the movement of deuterated tracers into polymer films.[12−18] Here we will demonstrate the use of SIMS to measure the detailed diffusion profile of deuterium-labeled PS (dPS) into a precrystallized isotactic PS (iPS) matrix. Similarly to Quijada-Garrido et al., we observed a superposition of two Fickian diffusion profiles, one of which appears to dominate at the surface. As suggested by Van Alsten et al.,[3] the surface dominant diffusion mechanism occurs to saturate the amorphous pockets of the matrix near the tracer interface. We will show that the second mechanism follows the entropic barrier diffusion model, occurring as chains explore the bottlenecks between lamellae in the matrix. We will demonstrate that the $D \sim N^{-1}$ prediction for entropic barrier diffusion applies to this case of tracer diffusion into a semicrystalline matrix.

Experimental Section

Isotactic polystyrene, iPS, with number-average degree of polymerization, $N_i = 5400$ (as provided by Pressure Chemical in powder form), was melt pressed into films (~50 μm thick) between sheets of Kapton polyimide at 300 °C under a force of 40 psi and then rapidly quenched to room temperature. Van Alsten et al. report that this iPS sample is polydisperse in that 20% of the chains have $N_i < 10^3$. A 5 cm × 5 cm piece of the resulting translucent, flexible film was then allowed to crystallize by annealing in a vacuum oven (10^{-3} Torr) at 180 °C for 4 h. The resulting film was opaque and brittle.

Table 1. Summary of Tracer Molecular Weights, Polydispersities, and Diffusion Times Used in This Study

N	$\bar{M}_w$	$\bar{M}_w/\bar{M}_n$	diffusion time (h)
91.4	9 500	1.04	1.25
			2
250	26 000	1.03	4.5
			5.75
814	90 000	1.02	7.25
			5
1125	117 000	1.03	7.25
			4
5480	570 000	1.06	10
			8

Small-angle X-ray scattering (SAXS) was performed at the Material Research Laboratory X-ray Facility at UCSB on the crystallized thin films to determine the lamellar long period of the crystallites. Copper Kα radiation with wavelength 1.54 Å was generated by a fine focus (0.2 mm) Rigaku rotating anode generator. The beamline was configured with a spot size of approximately 1 mm × 1 mm which was transmitted through the Kapton windows of the cell. Scattering patterns were collected on a Bruker HI-STAR multiwire area detector located 1.5 m from the sample. The peak scattering position, q^*, was located at $q = 0.49$ nm^{-1} (full width, half-maximum of 0.2 nm^{-1}), corresponding to a lamellar long period of 12.8 nm. This measurement is comparable to the long period of 13.9 nm observed by Van Alsten et al. Polarized light microscopy revealed many birefringent (crystalline) arms typical of spherulitic structures. The overlaying of a few layers of spherulitic structures in our films made it impossible to distinguish individual spherulites and measure spherulitic size, but we assume they are of similar size to those observed by Van Alsten et al. (~60 μm). In a much more detailed study of the crystalline morphology and melting behavior of the identical iPS crystallized under the same conditions, Van Alsten et al.[19] report dual-population melting behavior above 200 °C. Their DSC calorigrams, which depict two strong melting peaks at 209 and 218 °C, and microscopy studies suggest the presence of high melting, highly ordered crystallites surrounded by less ordered, volume-filling crystallites formed later in the crystallization.

To perform diffusion and SIMS experiments, it was necessary to attach the brittle films to a more durable support. Silicon substrates were obtained from Cypress Semiconductor Corp. (Minneapolis, MN), and a 300 nm thick layer of silicon oxide was deposited on the wafer via electron beam evaporation. The SiO_2 substrate layer serves to insulate the overlying polymer layer so that charge neutralization conditions using a low-energy electron gun in the SIMS crater do not change as the crater approaches the polymer/substrate interface. The iPS film was then broken into smaller pieces (0.25 cm^2), and each piece was affixed to a solid silicon wafer support using ethyl 2-cyanoacrylate (Elmer's Super Glue).

Perdeuterated, atactic polystyrene (dPS) samples as specified in Table 1 were obtained from Polymer Laboratories. Additional dPS samples were synthesized as previously documented.[15] The dPS was allowed to diffuse into the iPS matrix using the following procedure: The tracer layer was produced by spin-coating a thin film approximately 10 nm in thickness onto a glass slide. This film was then carefully floated off the glass slide on a deionized water bath and picked up on the thick iPS matrix film. The brittleness of films of low molecular weight dPS causes them to break up upon floating to the water surface. This floating procedure was therefore impractical for dPS layers with molecular weight less than 50 000 g/mol, so in these cases mixtures of 75% dPS and 25% high molecular weight hPS (2×10^6 g/mol) were substituted. It was assumed that the hPS was of high enough molecular weight as to diffuse only negligibly into the matrix during the time of the diffusion of the low molecular weight dPS.

Diffusion. The samples were then annealed under a He atmosphere at 160 °C for an appropriate length of time so that the total diffusion distance, L ($L = (Dt)^{0.5}$, using the short time

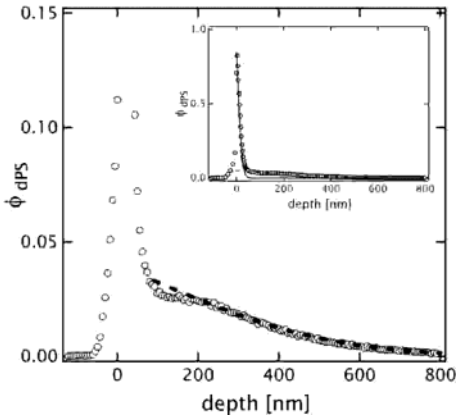

Figure 1. A representative depth profile showing the volume fraction dPS as a function of depth. The inset is the entire depth profile of a 90K dPS tracer film allowed to diffuse into the iPS matrix for 5 h at 160 °C in a helium environment. Open circles indicate the depth profile obtained from SIMS while the two lines indicate fits to two separate diffusion equations. The solid line visible in the inset is a fit of the interface profile with a diffusion coefficient of $D = 8 \times 10^{-17}$ cm^2/s. While this fit is acceptable within the interfacial region, it fails to fit the diffusion tail. The larger graph is a magnification of the diffusion tail to show its fit to a Fickian profile (eq 2) with $D = 3.9 \times 10^{-14}$ cm^2/s (dashed line).

diffusion coefficient from Van Alsten et al.[3] as an estimate), was approximately 0.5 μm. For each value of N, two diffusion times were sampled. In this manner, we were able to observe any deviation from the profiles resulting from non-Fickian diffusion processes. The annealing times ranged from 1 to 16 h. Upon removal from the oven, all samples still appeared opaque and smooth.

Dynamic SIMS. Prior to SIMS analysis, a sacrificial layer of hPS thin film (~60 nm thick) was spun-cast onto a glass microscope slide, floated off onto a distilled water bath, and picked up onto the specimen surface. This sacrificial layer was used to calibrate the etch rate of the SIMS. The sputtering was performed with a Physical Electronics 6650 dynamic SIMS using a 3 keV, 40 nA beam of O_2^+ ions rastered over a 0.09 mm^2 region. Charge neutralization was accomplished using a static, defocused, 1 keV electron beam. Negative ions of H, ^{2}H (D), C, and Si were monitored as a function of time from an electrically gated region in the center of the sputtered crater. This region is less than 20% of the rastered area.

Under such conditions, we obtain depth profiles with resolutions corresponding to a Gaussian with a full width half-maximum of ~15 nm. By measuring the thickness of the sacrificial PS layer via ellipsometry, we convert sputtering time to depth, assuming a steady rate of sputtering. Combining this depth scale with known information on the original concentration and thickness of the dPS layer, we are able to convert the intensities of negative ions into the volume fraction of dPS as a function of depth.

Results

A typical volume fraction vs depth profile for $N = 865$ after diffusion for 18 000 s at 160 °C is shown in Figure 1. This depth profile consists of a very high-concentration surface region and a low-concentration tail penetrating into the iPS to greater depths, as shown in the inset of Figure 1. The two different regions of the depth profile imply two different modes of dPS diffusion in the film. The initial very sharp peak is a surface layer which broadens very slowly by diffusion with a diffusion coefficient ~10^{-16} cm^2/s. This surface diffusion coefficient does not appear to be very dependent on tracer polymer molecular weight. The initial mutual diffusion of iPS into the tracer layer was previously observed by Van Alsten et al.[3]

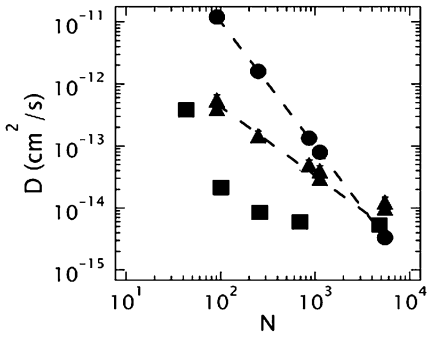

Figure 2. Comparison of the diffusion coefficient at 160 °C for dPS penetrants with degree of polymerization N into iPS matrices (triangles), into amorphous matrices from the data of Green and Kramer[21] (circles), and into iPS matrices as found by Van Alsten et al.[3] (converted to 160 °C using the WLF equation) (squares). The error bars on the diffusion coefficients, as determined by fitting each SIMS depth profile with a range of diffusion coefficients, are comparable to the sizes of the triangles.

From this higher concentration interfacial region, the dPS then diffuses into the bulk of the film, as shown in Figure 1. This second diffusion profile is well fit by a Fickian profile if it is assumed that the interface concentration in the iPS just under the tracer layer remained at constant interface concentration, C_0. Measurements at two different diffusion times for each sample confirms that C_0 is approximately constant. We therefore model this diffusion tail as diffusion into a semiinfinite medium from a boundary kept at a constant concentration. The dashed line of Figure 1 represents a fit to the solution of the diffusion equation:[20]

$$C(x) = C_0 \operatorname{erfc} \frac{x}{2\sqrt{Dt}} \qquad (2)$$

Here D is the diffusion coefficient, x is the distance from the surface, and t is the annealing time. The result from eq 1 was convoluted with a Gaussian (full width half-maximum = 15 nm) which represents the instrumental depth resolution of SIMS. The SIMS data were then fit by varying both D and C_0 to obtain the dashed line fit to the experimental data (circles) in Figure 1.

The diffusion tail profiles were fit for all the samples in this manner. In all cases, there was a near exact match of the diffusion coefficients for the two annealing times for each sample. In Figure 2, the diffusion coefficients are plotted as a function of tracer molecular weight. Also presented are the diffusion coefficients obtained from infrared ATR spectroscopy by Van Alsten et al.[3] (Figure 11 of this paper) which have been shifted from their experimental conditions of 170 °C to a temperature of 160 °C using the WLF equation, so that it may be compared to the results of these SIMS experiments. The previous study indicates that the diffusion coefficient decreases and then plateaus as a function of tracer size. This is not true in our case; in fact, the higher molecular weight tracers seem to follow the same power law dependence on N as the first two points. The diffusion coefficients, as calculated from the SIMS depth profiles, decrease algebraically with N, and a best fit is shown as a dashed line in Figure 2 with a slope of −0.91.

Van Alsten et al. measured the amount of tracer still remaining with the evanescent infrared wave of an attenuated total reflection infrared spectroscopy silicon crystal element. As mentioned earlier, by measuring the

long-range diffusion of iPS into dPS with this integral method, they did not observe a power law dependence of D on N when calculating D. Instead, they observed the mutual diffusion of the tracer and amorphous matrix chains and a corresponding weakening of the dependence of D on N as the tracer size was increased.[3] Using SIMS, we were only able to measure diffusion over much shorter times than Van Alsten et al. with much greater detail. We obtained the diffusion coefficients by directly fitting the depth profile with a solution to Fick's equation and were therefore able to distinguish the two separate diffusion profiles in our depth profiles. As a result, we observed both the mutual diffusion that saturated the skin of the iPS matrix and the diffusion that occurs as dPS chains explored the bottlenecks between lamellae.

Also plotted in Figure 2 are the expected diffusion coefficients for dPS tracers diffusing into an atactic polystyrene matrix melt consisting of very long chains from the data of Green and Kramer.[21] They found that diffusion in this regime followed the prediction of reptation such that the diffusion of a tracer into a matrix consisting of very long chains is dependent only on the molecular weight of the tracer, the monomeric friction coefficient, the entanglement molecular weight, and temperature. As seen in Figure 2, this case of diffusion into amorphous polystyrene follows the expected N^{-2} dependence predicted by reptation. A crossover is observed at high molecular weights where diffusion into the semicrystalline matrix is comparable to that into the high molecular weight amorphous matrix.

For $N \leq 10^3$, we observe that the diffusion of tracer dPS through a semicrystalline matrix is slower than that through a comparable amorphous matrix and that $D \sim N^{-1}$. Both of these observations are in good agreement with the predictions for entropic barrier diffusion around randomly spaced obstacles. In this case, the tracer molecules are atactic and cannot be incorporated into the crystalline domains. Regions in the crystalline domains with slight fluctuations in lamellar spacing which cause constrictions in the amorphous regions or with greater densities of tie chains create obstacles around which the dPS must diffuse.

When N approaches 10^4, we observe that the diffusion coefficients for the amorphous and semicrystalline matrices become comparable. At this high tracer molecular weight, the obstacles presented by the lamellar structures may no longer affect the tracer chains individually. The chains are responding to an averaged environment and reptating around lamellar obstacles. It is not surprising, therefore, that the numerical value of the diffusion coefficients for the amorphous and semicrystalline matrix cases are very similar at this point. It is expected that if the tracer size is increased to be much greater than the characteristic length scale of the obstacle structure, the slope in log D vs log N would cross over to -2 to reflect the reptation occurring in the system. While experiments conducted with larger tracers (higher N) might demonstrate this crossover, these experiments are further complicated due to the increased likelihood of phase segregation due to deuteration effects as the tracer size is increased. Furthermore, Pressure Chemical no longer produces the iPS used in this study, so further experiments are not possible until a new source of iPS can be identified.

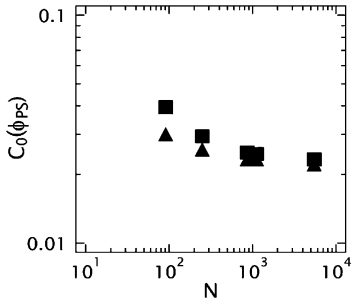

Figure 3. Extrapolated surface concentration as a function of the degree of polymerization of dPS. Squares represent shorter diffusion times while triangles indicate longer diffusion times.

In the crystallization process, low molecular weight and/or less isotactic material is rejected from the growing spherulites by fractionation.[22,23] These polymer molecules possess sufficient mobility in the melt to diffuse away radially in advance of the growing spherulites and remain in the interfibrillar regions. While there is no well-defined molecular weight above which all molecules are crystallizable, the probability of rejection from the growing spherulite becomes appreciable, in most cases, between 5000 and 10 000 g/mol. The reported polydispersity[3] of the iPS indicates that approximately 20% of the matrix polymer is comprised of chains below $N = 10^3$. As a result, the average molecular weight of matrix encountered by the dPS tracer in the interlamellar regions may be quite low. As a result, it is not surprising that the diffusion coefficient measured for diffusion of very high molecular weight ($N > 10^4$) dPS into semicrystalline iPS is slightly faster than that into the corresponding amorphous matrix.

The concentration at the interface can be estimated as the extrapolated surface concentration (where the dashed line in Figure 1 plateaus). This information is presented as Figure 3, with values for both time sets of each tracer molecular weight represented. The interface concentration, C_0, is very low, indicating that the solubility of dPS in iPS is also minimal. Microscopic observations by Van Alsten et al. suggest that many of the iPS lamella are connected together. In this case, the dPS solubility may be primarily limited by the topology of the crystalline regions producing inflexible interlamellar volumes. Thus, solubility would be limited by available interlamellar volume exchangeable between the low MW (uncrystallized) iPS and dPS. Alternatively, the atactic material may be absorbed into the interlamellar spacings, and as these regions swell, the iPS tie chains are stretched. This stretching may create an entropic mixing penalty which limits the solubility of dPS into the semicrystalline matrix.

The value of C_0 is only very weakly time dependent, indicating that the saturation of the surface layer is not only immediate but that it is continually replenished. We can conclude, therefore, that our assumption of constant concentration at the interface for the aforementioned Fickian fits was reasonable. The surface concentration of lower tracer molecular weight samples appears to decrease slightly with time, indicating that the diffusion away from the interface is occurring slightly faster than the interface can be replenished. Further, the saturation concentration decreases with increasing size of the dPS. This indicates, as expected, that the immediate uptake of tracer to the interface is N dependent and plateaus at $N = 1000$. At this point,

interdiffusion of the noncrystallizable fraction of the iPS matrix polymer into the tracer layer may be responsible for the broadening of the dPS layer as seen through SIMS. This interdiffusion is not expected to be highly dependent on the molecular weight of the tracer dPS layer.

Conclusions

Using SIMS, we generate depth profiles detailing the movement of deuterated tracers into a precrystallized polymer film. By directly fitting these curves with Fickian diffusion equations, we observe two distinct diffusion profiles. Near the surface, we see mutual diffusion of the surface iPS chains and tracer chains that acts to saturate this interface. From this constant composition interface, we observe a diffusion tail extending far into the iPS matrix. While the mutual diffusion occurring at the surface appears to be constant with tracer size, the Fickian diffusion coefficient associated with the diffusion tail has a $D \sim N^{-1}$ dependence. This diffusion behavior in the tail is suggestive of entropic barrier diffusion which occurs as the dPS chains explore the bottlenecks between lamellae.

Acknowledgment. This work was supported by the MRSEC Program of the National Science Foundation under Award DMR00-8003, the MRL Research Experience for Teachers Program (A.J.), and the Corning Foundation Fellowship of the MRL (R.A.S.). The able assistance of Tom Mates for SIMS and Ryan C. Hayward for SAXS is also greatly appreciated.

References and Notes

(1) Van Alsten, J. G.; Lustig, S. R. *Macromolecules* **1992**, *25*, 5069−5073.
(2) Lustig, S. R.; Van Alsten, J. G.; Hsiao, B. *Macromolecules* **1993**, *26*, 3885−3894.
(3) Van Alsten, J. G.; Lustig, S. R.; Hsiao, B. *Macromolecules* **1995**, *28*, 3672−3680.
(4) Quijada-Garrido, I.; Barrales-Rienda, J. M.; Frutos, G. *Macromolecules* **1996**, *29*, 7164−7176.
(5) Billingham, N. C.; Calvert, P. D.; Uzuner, A. *Polymer* **1990**, *31*, 258−264.
(6) Muthukumar, M.; Baumgartner, A. *Macromolecules* **1989**, *22*, 1937−1941.
(7) Muthukumar, M.; Baumgartner, A. *Macromolecules* **1989**, *22*, 1941−1946.
(8) Zimm, B. H.; Lumpkin, O. *Macromolecules* **1993**, *26*, 226−234.
(9) Turner, S. W. P.; Cabodi, M.; Craighead, H. G. *Phys. Rev. Lett.* **2002**, *88*, 128103/1−128103/4.
(10) Nykypanchuk, D.; Strey, H. H.; Hoagland, D. A. *Science* **2002**, *297*, 987−990.
(11) Smisek, D. L.; Hoagland, D. A. *Science* **1990**, *248*, 1221−1223.
(12) Zheng, X.; Rafailovich, M. H.; Sokolov, J.; Zhao, X.; Briber, R. M.; Schwarz, S. A. *Macromolecules* **1993**, *26*, 6431−6435.
(13) Zheng, X.; Sauer, B. B.; Van Alsten, J. G.; Schwarz, S. A.; Rafailovich, M. H.; Sokolov, J.; Rubinstein, M. *Phys. Rev. Lett.* **1995**, *74*, 407−410.
(14) Zheng, X.; Rafailovich, M. H.; Sokolov, J.; Strzhemechny, Y.; Schwarz, S. A.; Sauer, B. B.; Rubinstein, M. *Phys. Rev. Lett.* **1997**, *79*, 241−244.
(15) Yokoyama, H.; Kramer, E. J.; Rafailovich, M. H.; Sokolov, J.; Schwarz, S. A. *Macromolecules* **1998**, *31*, 8826−8830.
(16) Yokoyama, H.; Kramer, E. J.; Hajduk, D. A.; Bates, F. S. *Macromolecules* **1999**, *32*, 3353−3359.
(17) Yokoyama, H.; Kramer, E. J. *Macromolecules* **2000**, *33*, 1871−1877.
(18) Pu, Y.; White, H.; Rafailovich, M. H.; Sokolov, J.; Patel, A.; White, C.; Wu, W. L.; Zaitsev, V.; Schwarz, S. A. *Macromolecules* **2001**, *34*, 8518−8522.
(19) Van Alsten, J. G.; Lustig, S. R.; Hsiao, B. *Macromolecules* **1995**, *28*, 3672−3680.
(20) Crank, J. *The Mathematics of Diffusion*, 2nd ed.; Clarendon Press: Oxford, England, 1993.
(21) Green, P. F.; Kramer, E. J. *J. Mater. Res.* **1986**, *1*, 202−204.
(22) Keith, H. D.; Padden, F. J. *J. Appl. Phys.* **1964**, *35*, 1270−1286.
(23) Keith, H. D.; Padden, F. J. *J. Appl. Phys.* **1964**, *35*, 1286−1298.

MA035705A